RUSSIAN JOURNAL OF EARTH SCIENCES, VOL. 3, NO. 3, PAGES 219–234, AUGUST 2001

Magmatic amphiboles and micas in oceanic peridotites and some specific features of the related magmas: 15°20′ N MAR Fracture Zone

B. A. Bazylev[1], S. A. Silantiev[1], H. G. B. Dick[2], and N. N. Kononkova[1]

[1]Vernadskii Institute of Geochemistry and Analytical Chemistry, Russian Academy of Sciences
[2]Woods Hole Oceanographic Institution, MacLean Laboratory, USA

Abstract. The aim of this work was to study the petrography and mineralogy of mineral associations with magmatic high-Ti hornblendes and micas in MAR spinel harzburgite. The mineral compositions were examined using electron and ion microprobes. It was found that these mineral associations had been formed in a temperature range of 870–950°C as a result of the crystallization of a residual highly differentiated (96–98%) mantle magma and its interaction with the host peridotite. Based on the compositions of the pyroxenes and amphibole, the initial mantle magma was in equilibrium with the minerals of the restite harzburgite and based on its enrichment in LREE (La/Sm_N = 10–12) can be classified as intraplate OIB magma. The absence of a Sr anomaly in the model composition of the initial magma, evaluated for one of the two MAR areas concerned (Site 16ABP-68), and the negative Sr anomaly characteristic of the model composition of the magma, calculated for the other MOR area (Site 16ABP-62), can serve as an independent confirmation of the local rock heterogeneity in the region of intraplate magma generation, possibly associated with a crustal component recycling.

Introduction

Biotite and hornblende are rather often found in oceanic gabbroids and more silicic plutonic rocks which are usually classified as vein formations [*Cannat and Casey,* 1995; *Cannat et al.,* 1992; *Silantiev,* 1998]. Micas and hornblendes are more rare in abyssal peridotites, especially in those of restite origin, than in plutonic rocks of basic and acid composition. Two alternative mechanisms have been proposed for the crystallization of these minerals in the rocks of the 3d layer of oceanic crust: a magmatic mechanism (from highly differentiated magmas) (e.g., [*Arai and Matsukage,* 1996; *Arai et al.,* 1997]) and a metamorphic mechanism associated with the hydrothermal sea water circulation under mid-oceanic ridges (e.g., [*Cannat and Casey,* 1995; *Silantiev,* 1998])

Copyright 2001 by the Russian Journal of Earth Sciences.

Paper number TJE01066.
ISSN: 1681–1208 (online)

The online version of this paper was published October 18, 2001.
URL: http://rjes.agu.org/v03/TJE01066/TJE01066.htm

Earlier [*Bazylev et al.,* 1999], we showed that amphiboles and micas in oceanic spinel peridotites were of different origins related to different sources of water. These sources might be sea water percolating to deep crustal rocks or magma rising from the mantle and its juvenile aqueous fluids.

The aim of this study was to derive new data on the compositions of micas and amphiboles in the mantle peridotites of the Mid-Atlantic Ridge (MAR), the crystallization of which was associated with magma. In the context of this problem we attempted to evaluate the potential compositions of the magmas that were in equilibrium with magmatic amphiboles and micas in the oceanic mantle restite and to reconstruct some of the magmatic parameters distinguishing the axial MAR zone between 14 and 15°N.

Tectonic Setting and Brief Description of Samples

The samples of the ultrabasic rocks examined in this study had been dredged from the crest of the Mid-Atlantic Ridge

(MAR) during cruise 16 of the R/V Akademik Boris Petrov. Given below are the brief descriptions of the dredging sites and the petrographic types of the rocks characteristic of them.

Dredging site ABP-16-62 (14°55′ N, 44°29′ W) was located on the southern side of the 15°20′ N fracture zone valley, in its passive part, east of its intersection with the southern segment of the rift valley. The peridotite samples collected at this site were represented by clinopyroxene-bearing spinel harzburgite (with Cr/(Cr+Al) = 0.36–0.49), locally highly schistose and mylonitized. All rocks are highly serpentinized. Some samples were found to contain large orthopyroxene grains (<2–3 mm in size) with clinopyroxene lamellae. Clinopyroxene is also present as scarce small xenomorphic grains at the edges of the orthopyroxene or bastite grains. Hornblende occurs as monomineral amphibolite veinlets (30 μm to 3 cm), conformable with schistosity in the schistose rocks, and also scattered grains (<0.3 mm) developed after olivine and orthopyroxene. No phlogopite was found in the peridotite of this site. Chrome spinellid is present as brownish grains, sometimes fringed with magnetite.

Sample 62-7 is mylonitized harzburgite containing a rather thick (3–5 mm) amphibole veinlet. The average size of individual amphibole grains in it is ca. 0.1 mm. Sample 62-8 is spinel harzburgite with a thin (0.05 mm) amphibole veinlet. Fine grains of amphibole (<0.05 mm) are disseminated in the completely serpentinized matrix of the rock. The sample was found to contain both large relict orthopyroxene grains (2 mm) and the neoblasts of this mineral (0.1 mm) developed near the amphibole veinlets. Sample 62-10 contains very small (<0.05 mm) round grains of clinopyroxene, localized mainly near the margins of the orthopyroxene grains. No amphibole was found in these rocks. Sample 62-11 is distinguished by the presence of a rather thick amphibole veinlet (>5 mm thick). The veinlet was found to contain an opaque chrome spinellid grain with signs of corrosion (0.3 mm), and also fine (~5 μm) interstitial grains of plagioclase (An_{39}) and apatite.

The peridotites raised by this dredge did not show any indications of magmatic vein formations of the gabbro or diorite appearance. However, gabbroids containing mica and showing an alkaline geochemical speciation were described earlier among the rocks dredged in this area [*Silantyev,* 1998].

Dredging site ABP-16-68 (14°49′ N, 45°05′ W) is the western slope of the rift valley south of 15°20′ N. This site is of particular interest because it is situated in the direct vicinity of the peak of a 14°48′ N geochemical anomaly. The peridotite dredged in this area is a relatively fresh clinopyroxene-bearing spinel harzburgite (Cr# = 0.48–0.60 in primary spinellid and Mg# = 91.7–92.3 in olivine). The rock preserved orthopyroxene grains as large as 5 mm. The chrome spinellid grains are reddish brown, some being opaque.

Hornblende occurs as fine (0.05–0.1 mm) colorless rounded dispersed grains restricted to the margins of large bastitized orthopyroxene grains where pyroxene associated with amphibole was not preserved. Clinopyroxene is either dispersed in the matrix or restricted to the marginal parts of bastitized orthopyroxenes and is indistinguishable petrographically from the hornblende. Portions of orthopyroxene hosting clinopyroxene were found to be preserved in Samples 68-14 and 68-19. Hornblende grains were found in olivine, outside of orthopyroxene, in Sample 68-19.

Scarcely scattered colorless phlogopite flakes (<0.05 mm) are often associated with hornblende and orthopyroxene (e.g., in Sample 68-2). One of the hornblende grains in the olivine of Sample 68-3 was found to contain a small (5μm) round rutile inclusion.

Some hartzburgite samples contain igneous rock veinlets. In Samples 68-8, 68-18, 68-19, and 68-27 they are as thick as e few centimeters and are represented by diorite composed of brown hornblende grains (<1.5 mm), brown biotite flakes (<0.8 mm), plagioclase (usually completely prehnitized), and numerous grains of ilmenite, zircon, and apatite. The margins of the brown hornblende grains consist of greenish or colorless amphibole which also occurs as individual prismatic grains, especially abundant at contacts between diorite and hartzburgite, where greenish biotite and talc are associated with amphibole.

An igneous rock veinlet in Sample 68-37 (1.5 mm thick) is represented by gabbro norite and is composed in the central part of plagioclase (An_{41}), clinopyroxene (Table 1, #10), orthopyroxene (Table 1, #18), and scarce small zircon grains. Closer to the edge, plagioclase grows more basic (An_{56-79}) and is associated only with orthopyroxene. The contact zone has a monomineral composition and consists of orthopyroxene or of orthopyroxene with colorless hornblende. Locally, the outer contact of the veinlet shows occasional portions composed of brown hornblende and plagioclase.

The host hartzburgite contains small (<0.1 mm) grains of colorless hornblende (Table 2, #11) restricted to a contact between orthopyroxene (Table 1, #17) and clinopyroxene (Table 1, #9) in the vicinity of spinel (Table 3, #7). Also found in this area are contacting pyroxenes without hornblende in the contact zone (Table 1, #8 and 16).

Analytical Methods

The contents of major elements in the minerals were determined on a CAMECA CAMEBAX electron microprobe at the GEOKhI RAN, Moscow, using an acceleration voltage of 15 kV and a microprobe current of 35 nA. The duration of analysis was 10 s for Si, Ti, Al, Fe, Mg, Ca, and Na and 30 s for Mn, Ni, V, Zn, Cl, and K. Measurements were made with a beam size of 1–2 μm. The compositions of the cores of large orthopyroxenes were measured using rasters of 5×5 and 12.5×12.5μm to eliminate the effects related to exsolution. Natural minerals (PYR21 pyroxene, OLC1 olivine, and UV126 spinel [*Lavrentiev et al.,* 1974]) and synthetic minerals were used as standards. The accuracy of one-point measurements was characterized by a standard deviation (σ, wt%) which depended on the element analyzed and on its content in the mineral (x, wt%). The empirical relation be-

Table 1. Representative compositions of pyroxenes

#	1*	2*	3	4*	5*	6*	7	8	9
Sample	62-10	62-12	Dr68av	68-11	68-14	68-19	68-2	68-37	68-37
Generation	Cpx_1	Opx_1	Cpx_1/O	Cpx_1/O	Cpx_1/O	Cpx_1/O	Cpx_1/O	Cpx_1/O	Cpx/H
Sites	7	2	35	3	7	6	2	4	6
SiO_2	53.52	56.21	53.67	53.88	53.44	54.18	53.79	53.67	54.49
TiO_2	0.07	0.02	0.08	0.03	0.09	0.06	0.14	0.18	0.14
Al_2O_3	1.98	2.56	2.33	2.33	2.16	2.14	2.00	2.32	1.77
FeO	2.47	5.70	1.88	1.89	1.85	1.81	2.05	2.03	2.02
MnO	0.05	0.09	0.05	0.05	0.06	0.06	0.04	0.05	0.05
MgO	17.60	32.85	17.18	16.93	17.63	17.43	18.75	17.43	17.36
CaO	22.16	1.07	22.60	22.50	22.52	23.09	21.65	22.87	23.76
Na_2O	0.34	0.02	0.42	0.46	0.44	0.37	0.45	0.35	0.26
Cr_2O_3	0.65	0.66	1.24	1.42	1.12	1.11	1.08	1.02	0.85
NiO	NA	NA	NA	NA	NA	NA	NA	NA	NA
Total	98.83	99.17	99.47	99.49	99.30	100.25	99.93	99.95	100.73
Mg#	92.6	91.1	94.2	94.1	94.5	94.5	94.2	93.9	93.9
W77	996		946	945	970	930	1056	950	882
BK90/C	965		929	948	931	897	1029	916	831
BK90/O		1020							
WS91		989							

#	10	11	12	13*	14	15	16	17	18
Sample	68-37	dr68av	dr68av	68-2	68-2	68-3	68-37	68-37	68-37
Generation	Cpx/GV	Opx_1S	Opx_1/C	Opx_1/C	Opx/H.P	Opx/H	Opx_1/C	Opx/H	Opx/GV
Sites	9	20	11	10	6	4	3	5	6
SiO_2	53.44	57.29	56.99	57.70	58.51	57.66	57.09	58.00	56.05
TiO_2	0.30	0.04	0.03	0.09	0.22	0.25	0.08	0.07	0.10
Al_2O_3	1.15	2.18	1.94	1.87	1.14	1.38	1.75	1.51	0.66
FeO	8.71	5.21	5.10	5.39	5.60	5.36	5.75	5.86	15.28
MnO	0.31	0.12	0.12	0.13	0.13	0.13	0.16	0.13	0.36
MgO	15.30	33.02	33.95	34.01	34.48	34.27	34.74	34.10	27.87
CaO	20.87	2.11	0.78	0.63	0.57	0.82	0.78	0.68	0.92
Na_2O	0.33	0.05	0.03	0.04	0.03	0.03	0.03	0.01	0.06
Cr_2O_3	0.07	0.78	0.68	0.64	0.19	0.25	0.47	0.46	0.05
NiO	NA	NA	NA	NA	NA	NA	NA	NA	NA
Total	100.50	100.80	99.61	100.50	100.87	100.13	100.85	100.82	101.36
Mg#	75.8	91.8	92.2	91.8	91.7	91.9	91.5	91.2	76.5
W77	981								
BK90/C	957								
BK90/O		1216	943	895	>874	>954	941	911	989
WS91		1016	969	947	>746	>775	880	863	>684

Note. Cpx = clinopyroxene; Opx = orthopyroxene, subscript 1 denotes primary composition (unaltered during hornblende and phlogopite crystallization); S is potential solidus composition; C denotes grain core; R, grain rim; GV, gabbro veinlet; GDV, gabbro-diorite veinlet; /H, /P, /O, and /C denote generations in contact with hornblende, phlogopite, orthopyroxene, and clinopyroxene, respectively. Temperature estimates (°C): W77 – two-pyroxene Ca-Mg geotherm ometer [*Wells*, 1977]; BK90/C and BK90/O – clinopyroxene and orthopyroxene Ca-Mg geothermometers [*Brey and Köhler*, 1990] (where another equilibrium pyroxene was absent the value was the lower limit); WS91 – orthopyroxene-olivine-spinel Cr-Al geothermometer [*Witt-Eickschen and Seck*, 1991] (where equilibrium chrome spinellid was absent the value was the lower limit).

Table 2. Representative compositions of hornblendes

#	1	2*	3*	4	5*	6*	7	8	9	10	11
Sample	68-2	68-2	68-3	68-3	68-8	68-14	68-22	68-27	68-37	68-37	68-37
Generation	/O	/O, P			DV		/P	DV	GDV	GDV	/O, C
Mineral	Parg	Ed	Ti-Parg	Parg	Ti-Ed	Ed	Ed	Ti-Ed	Ed	Ed	Ed
Sites	4	4	3	6	2	2	6	2	2	6	6
SiO_2	46.25	47.23	44.38	45.21	46.21	46.77	46.24	45.61	47.17	47.01	48.51
TiO_2	1.80	1.98	2.74	1.97	2.36	0.40	1.23	2.40	0.90	0.93	0.62
Al_2O_3	12.70	12.09	12.73	12.40	8.58	10.73	12.02	8.52	11.06	12.76	10.28
FeO	2.84	3.01	3.04	2.81	16.18	2.55	2.79	18.28	4.60	3.01	2.89
MnO	0.05	0.07	0.07	0.06	0.20	0.07	0.07	0.20	0.11	0.07	0.04
MgO	18.93	19.37	18.56	18.46	12.59	19.49	19.20	11.51	19.54	19.74	19.66
CaO	11.73	11.72	11.79	12.60	10.45	12.08	11.42	10.45	11.20	11.68	12.56
Na_2O	2.61	2.49	2.64	2.50	2.31	2.33	2.51	2.16	2.42	2.74	2.20
K_2O	0.40	0.36	0.38	0.54	0.41	0.16	0.38	0.47	NA	0.21	0.10
Cr_2O_3	2.04	0.51	1.40	1.68	0.00	2.05	1.19	0.06	1.27	0.53	1.94
NiO	NA	NA	NA	NA	NA	NA	0.05	NA	NA	NA	NA
Total	99.34	98.84	97.74	98.22	99.29	96.62	97.10	99.65	98.28	98.77	98.81
Cl	0.10	0.11	0.10	0.13	0.07	0.02	0.11	0.08	NA	0.02	0.01
Mg#	92.2	92.0	91.6	92.1	58.1	93.2	92.5	52.9	88.3	92.1	92.4

Note. GDV – gabbro-diorite veinlet; DV – diorite veinlet; /P, /O, /C – generations at an immediate contact with phlogopite, orthopyroxene, and clinopyroxene, respectively. Amphibole varieties are given in accordance with the classification of [*Leake et al.*, 1997]: Parg = pargasite, Ed = edenite, Ti- = titaniferous.

Table 3. Representative compositions of chrome spinellids

#	1	2	3	4	5	6	7	8	9	10
Sample	dr62av	dr62av	62-7	62-7	Dr68av	68-37	68-37	68-37	68-37	68-37
Generation	Spl_1	Spl_1R	/H, O	V/H, Pl	Spl_1	Spl_1	Spl_2/H	Spl_2	Spl_2	Spl_2
D, mm			1.3	−0.8		>7.0	3.1	2.2	1.6	0–0.6
Sites	16	10	2	2	40	6	5	7	16	5
SiO_2	0.04	0.13	0.07	0.05	0.08	0.17	0.12	0.08	0.11	0.08
TiO_2	0.08	0.07	0.06	1.02	0.09	0.04	0.21	0.04	0.14	1.07
Al_2O_3	30.47	29.94	25.70	19.21	24.02	28.59	25.05	27.81	24.43	21.50
FeO	16.39	19.75	24.44	32.51	16.12	16.36	16.91	18.36	22.62	25.16
MnO	0.18	0.19	0.22	0.25	0.19	0.19	0.25	0.25	0.29	0.30
MgO	14.65	12.98	10.24	7.15	14.02	14.01	13.48	13.09	10.51	9.48
Cr_2O_3	37.72	35.89	39.04	39.54	44.78	39.05	43.65	39.61	41.49	41.66
NiO	NA	NA	0.15	0.29	0.10	0.07	0.08	0.10	0.10	0.13
V_2O_3	NA	NA	0.24	0.16	0.12	0.16	0.23	0.16	0.17	0.21
ZnO	NA	NA	0.32	0.38	0.14	0.22	0.16	0.19	0.34	0.27
Total	99.53	98.95	100.48	100.56	99.65	98.85	100.14	99.69	100.20	99.86
Cr#	0.454	0.446	0.505	0.580	0.556	0.478	0.539	0.489	0.533	0.565
Mg#	0.646	0.581	0.475	0.342	0.639	0.631	0.610	0.593	0.490	0.442
Fe#	0.026	0.039	0.055	0.109	0.026	0.022	0.020	0.030	0.040	0.052
Ol Mg#	NO	NO	NO	NO	92.3	91.7	91.5	91.2	89.1	86.6
BBG91					772	726	753	704	684	749
$lmfO_2$					−0.2	−0.4	−0.8	0.0	0.2	0.2

Note. D is the distance from diorite or amphibole veinlet; Cr# = Cr/(Cr+Al), M# = Mg/(Mg+Fe^{2+}), Fe# = Fe^{3+}/(Cr+Al+Fe^{3+}), Ol Mg# = 100*Mg/(Mg+Fe) of olivine coexisting with spinellid; BBG91 and $lmfO_2$ are the temperature (°C) and oxygen fugacity (in log units relative to buffer QFM), respectively, after [*Ballhaus et al.*, 1991]; NO – no olivine relics preserved; av – average compositions of peridotites from one dredge sample; Spl_1 – primary chrome spinellid; Spl_2 – secondary (recrystallized) chrome spinellid; C – grain core; R – grain rim; V – grain in amphibole veinlet; /H, /Pl, /O – generations in associations with hornblende, plagioclase, and orthopyroxene, respectively.

tween σ and x was

$$\log \sigma = (0.6 \times \log(x) - 1.4)) \pm 0.15 \qquad (1)$$

for all elements except Na and Mg with their contents in the mineral above 0.6 wt% of the oxide, and $\sigma = 0.03$ for the lower contents. The accuracy was slightly worse for Na and Mg.

The contents of REE and minor elements in the minerals were determined by the method of secondary ion mass spectrometry (SIMS) on a Cameca IMS-4f ion microprobe in the Institute of Microelectronics, Yaroslavl, Russia. The measurement procedure was similar to that described in [*Sobolev,* 1997]. The contents of elements were determined using a ratio between the contents of the most representative isotope and ^{30}Si isotope. The calibration curves were plotted from the results of measuring 15 natural glasses and clinopyroxenes, the compositions of which had been attested using the methods of isotope dilution and inductively coupled plasma atomic emission spectrometry (ICPES). The microprobe current was 5–7 nA, and the diameter of the focused beam was varied within 10–40 μm. To minimize the effect of complex ions, the energy was filtered with an offset of 100 eV. The content of europium was calculated from the results of measuring the contents of isotopes 151 and 153 to avoid the effect of BaO [*Johnson et al.,* 1990]. No special corrections were made for the effect of complex ions in water-bearing minerals. The accuracy of the measurements was not less than ±20% for most of the measured elements in clinopyroxenes and hornblendes, as well as for Ti, Zr, Li, Sr, Ce, and Y in orthopyroxenes. The accuracy was not lower than ±20% for most of the elements measured in clinopyroxenes and hornblendes and for Ti, Zr, Li, Sr, Ce, and Y, in orthopyroxenes. The accuracy was not worse than ±40% for the other elements. The REE contents in some clinopyroxenes were determined on a Cameca IMS-3f ion microprobe in the Woods Hole Oceanographic Institution, Ma, USA, using a conventional procedure [*Johnson et al.,* 1990; *Shimizu and Hart,* 1982].

Major Stages of Mantle Peridotite Recrystallization

The rocks under study are characterized by changes in the compositions of minerals, typical of abyssal spinel peridotites, and associated with the reactions that take place during the cooling of a mantle material after the separation of magmatic melt from it:

$$\begin{aligned}&(\mathrm{Al,Cr})-\text{rich Px} + \mathrm{Ol} \;=\\ &= \;(\mathrm{Al,Cr})-\text{poor Px} + \mathrm{Cr}-\text{Spinel}\,,\end{aligned} \qquad (2)$$

$$\mathrm{Ca}-\text{rich Opx} = \mathrm{Ca}-\text{pure Opx} + \mathrm{Ca}-\text{rich Cpx}\,. \qquad (3)$$

These mineral-formation reactions, operating in abyssal peridotites were described earlier in [*Arai and Fujii,* 1978; *Dick,* 1989; *Fujii,* 1990; *Hamlin and Bonatti,* 1980; *Juteau et al.,* 1990] and are used in the geothermometry of the processes of mantle rock recrystallization.

Petrographically, reaction (1) manifests itself in the crystallization of xenomorphic chrome spinel grains at the orthopyroxene-olivine contact and is accompanied by the decline of Al and Cr contents from the core of a pyroxene grain to its margin. Reaction (2) manifests itself in the exsolution of pyroxene and in the development of clinopyroxene lamellas in the orthopyroxene matrix, the lamellas tending to recrystallize to isometric grains usually confined to intergranular contacts. This reaction is accompanied by a decline in the content of Ca in orthopyroxene from the centers of large grains (when the matrix is analyzed together with the lamellas) to the margins and their neoblasts, where lamellas are absent, and the Ca contents are close to the Ca content in the matrix of the cores of orthopyroxene grains at the contacts with clinopyroxene lamellas. Near large chrome spinelid grains the compositions of silicates underwent abnormal impoverishment in iron, caused by subsolidus Fe-Mg redistribution. In this paper we use the term "primary mineral" for the mineral phases of mantle peridotites (olivine, pyroxenes, and chrome spinellid), which show these typical composition changes as a result of subsolidus reactions, as is typical of these rocks (e.g., [*Dick,* 1989; *Juteau et al.,* 1990]). The above comments, however, do not mean that these minerals were stable at solidus temperature, or that their compositions are consistent with the solidus ones.

The forms of clinopyroxene crystals in the studied peridotites indicate that it was not a solidus mineral. The cores of orthopyroxene porphyroblasts in the harzburgite from Sample 68, measured in a raster, showed elevated homogeneous contents of calcium, aluminum, and chromium. However in the hartzburgites of this dredge sample the contents of these elements showed a negative correlation with the average Cr content of the spinellid. Since the neoblasts of clinopyroxene and chrome spinellid are scarce around the large grains of orthopyroxene in the studied rocks, these compositional features of the orthopyroxenes may indicate that the cores of the orthopyroxene grains preserve the composition close to a solidus one (OpxS). On this basis a mass balance can be estimated for the reaction of subsolidus orthopyroxene recrystallization (3) in the harzburgite of dredge sample 68:

$$1.000\ \mathrm{OpxS} = 0.938\ \mathrm{Opx/C} + 0.062\ \mathrm{Cpx/O} \qquad (4)$$

where OpxS, Opx/C, and Cpx/O are the mean compositions of the minerals from Table 1 in wt%, with Opx/C and Cpx/O being the compositions of pyroxenes at the contact.

Where the olivine, pyroxenes, and chrome spinellid showed unusual compositions or were found to have a zonal pattern, which could not be explained by the above reactions (e.g. as a result of the reequilibration with the melt or of the reactions of hornblende or phlogopite crystallization), we use the term "secondary" for these minerals or their respective generations.

After the melt separation and subsolidus recrystallization some volume of the peridotite was intruded by basic and acid melts, which is manifested by the emplacement of gabbro

Table 4. Representative compositions of micas

#	1	2	3	4	5	6	7	8
Sample	68-2	68-2	68-8	68-18	68-19	68-22	68-27	68-37
Generation	/O, H	R	DV/H	DV	DV	/H	DV/H	GDV
Sites	3	2	5	4	2	2	3	4
SiO_2	39.48	39.18	40.44	40.68	36.93	40.79	37.22	41.35
TiO_2	2.07	1.64	1.55	3.07	2.67	2.29	4.31	0.98
Al_2O_3	16.36	15.65	13.31	13.27	13.54	16.16	14.21	17.45
FeO	2.93	4.47	7.57	8.41	16.05	2.91	19.92	2.84
MnO	0.04	0.04	0.03	0.07	0.07	0.10	0.09	0.03
MgO	23.62	24.93	22.46	21.65	16.79	24.23	14.18	24.78
CaO	0.17	0.38	0.14	0.13	0.01	0.23	0.35	0.03
Na_2O	1.56	0.64	0.34	0.35	0.37	1.64	0.30	0.60
K_2O	6.39	4.74	7.47	7.81	7.29	6.89	7.37	8.37
Cr_2O_3	0.23	0.12	0.69	0.03	0.09	0.66	0.10	0.52
NiO	NA	NA	0.20	NA	0.14	NA	NA	NA
Total	92.84	91.79	94.20	95.47	93.94	95.91	98.05	96.95
Cl	0.12	0.10	0.10	0.09	0.18	0.04	0.22	0.05
Mg#	93.5	90.9	84.1	82.1	65.1	93.7	55.9	94.0

Note. DV – diorite veinlet; GDV – gabbro-diorite veinlet; R - partially replaced grain; /O,/H – generations associated with orthopyroxene or hornblende, respectively; NA – not analyzed.

and diorite veinlets. The effect of these magmatic events on the mineralogy of the host peridotites is restricted to a rather narrow region, contacting the veinlets. In Sample 68-37 the Mg# of olivine grows gradually from 85.0 at the contact with a gabbro veinlet to 86.6 at a distance of 0.6 mm from the contact, to 89.1 at 1.6 mm, to 91.2 at 2.2 mm, to 91.5 at 3.1 mm, and to 91.7 at a distance of 7.3 mm and farther from the contact. The last value seems to mark the composition of olivine which was unaltered during the interaction with the late magma. Chrome spinellid showed a high Ti content (ca. 1 wt% of the oxide) only at the immediate contact with a veinlet, where it is accompanied by a decline in the Mg content. However, as close as 5 mm from the contact with the veinlet, chrome spinellid did not show any indications of interaction with the melt. At the contact with a diorite veinlet in Sample 68-18, the region of the alteration of primary minerals in peridotite is limited to an even more narrow interval: the Mg# of olivine grows from 75.5 at the contact to 89.0 at a distance of 0.25 mm from it, to 91.4 at 0.35 mm, to 91.8 at 0.4 mm, and to 92.5 at a distance of 0.8 mm and farther from the contact. Variations of the Mg# of olivine were found to be not accompanied by any systematic variations of the Ni and Ca contents in this mineral.

The next phase of peridotite recrystallization was associated with the crystallization of amphibole-bearing metamorphic mineral associations under the effect of hydrothermal fluids derived from sea water and circulating under mid-oceanic ridges.

At the highest temperature of this process hornblende is the sole aqueous mineral. For the hartzburgites under study we calculated amphibolization reactions balanced in terms of the major elements: Ca, Mg, Si, Al, and also Cr for reaction (6). According to the data for the harzburgite of Sample 68-37, the compositions of minerals (in wt%) were as follows:

$$13.782\ \mathrm{Opx/C} + 7.683\ \mathrm{Cpx/O} + 2.00\ \mathrm{wt.\%\ H_2O} + \\ + 1.04\ \mathrm{wt.\%\ Na_2O} = 1.000\ \mathrm{Hbl} + 12.804\ \mathrm{Opx/H} + \\ + 7.021\ \mathrm{Cpx/H} + 0.709\ \mathrm{Ol}\,, \quad (5)$$

where the source of alumina was primary pyroxene, and

$$11.420\ \mathrm{Opx/C} + 0.467\ \mathrm{Cpx/O} + 0.783\ \mathrm{Spl1} + \\ + 2.00\ \mathrm{wt.\%\ H_2O} + 1.80\ \mathrm{wt.\%\ Na_2O} = 1.000\ \mathrm{Hbl} + \\ + 10.361\ \mathrm{Opx/H} + 0.702\ \mathrm{Spl/H} + 0.662\ \mathrm{Ol}\,, \quad (6)$$

where the additional source of alumina was chrome spinellid.

At the lower temperature of the rocks this phase was accompanied by the development of tremolite, chlorite, and talc (and also prehnite in the gabbro and diorite veinlets). Hornblende, phlogopite, orthopyroxene, and plagioclase were replaced actively. The next phase of the rock recrystallization was serpentinization, during which serpentine replaced all primary and secondary peridotites, so that information of the metamorphic history was erased.

Composition of Rock-Forming Minerals

Major elements. Based on their Ti contents, the micas of the studied rocks can be classified into high-Ti micas (<0.62 wt% TiO_2), definitely nonmagmatic, and low-Ti

Table 5. Contents of REE and trace elements in minerals

#	1	2	3	4	5	6	7	8	9	10	11	12	13	14
Sample	68-11	68-14	68-14	68-2	68-2	68-3	68-14	68-8	68-8	68-18	68-19	62-10	62-12	62-12
Position	Hz	Hz	Hz	Hz	Hz	Hz	Hz	DV	DV	DV	DV	Hz	Hz	Hz
Mineral	Cpx	Cpx	Cpx	Opx	Hbl	Hbl	Hbl	Bi	Hbl	Bi	Bi	Cpx	Opx	Opx
Sr	5.3	3.6	NA	0.5	66.9	46.8	7.1	26.3	43.5	20.9	33.0	51.4	12.1	NA
Ba	1.74	0.75	NA	0.08	203	167	23.3	4730	131	2690	359	16.5	1.16	NA
Nb	0.35	0.19	NA	0.03	76	217	6.6	58.7	100	121	179	0.68	0.15	NA
Zr	9.55	4.74	NA	1.17	517	685	16.9	2.43	172	1.72	3.62	14.0	0.74	NA
Ti	462	338	NA	183	9460	10300	2210	10800	13900	18100	16900	412	342	NA
La	1.33	0.95	0.75	0.029	41.7	34.7	5.02	BDL	54.8	BDL	BDL	3.33	0.26	0.28
Ce	2.10	2.08	1.44	0.10	137	114	11.1	0.333	228	0.473	0.444	8.43	0.46	0.37
Nd	1.45	1.11	0.78	0.10	97.7	111	5.95	BDL	264	BDL	BDL	6.91	0.19	0.36
Sm	0.71	0.38	BDL	0.041	26.2	32.1	1.45	BDL	98.6	BDL	BDL	2.26	0.064	BDL
Eu	0.24	0.10	BDL	BDL	4.59	6.66	0.21	BDL	8.9	BDL	BDL	0.44	0.058	0.079
Dy	1.13	0.74	0.38	0.17	32.7	51.1	1.88	BDL	130	BDL	BDL	3.32	0.14	0.17
Er	0.56	0.33	0.27	0.19	18.5	27.2	1.04	BDL	68.0	BDL	BDL	2.14	0.20	0.38
Yb	0.53	0.31	0.31	0.30	17.5	22.0	0.99	0.15	67.3	0.12	0.09	1.66	0.31	0.46
Y	5.3	3.3	NA	1.2	165	241	10.6	0.32	540	0.32	0.19	16.5	1.5	NA
Li	5.2	3.2	NA	2.8	19.4	BDL	1.4	34	BDL	49	98	9.1	8.1	NA

Note. Hz – grain from spinel harzburgite; AV – grain from amphibole veinlet; DV – grain from diorite veinlet; Bi – biotite; Hbl – hornblende; Cpx – clinopyroxene; Opx – orthopyroxene; NA – not analyzed; BDL – content below experimental error. All contents are given in ppm. The contents of major elements are listed in Tables 2–4. Analyses 3 and 12 were made in the Woods Hole Oceanographic Institution, the others, in the Institute of Microelectronics (Yaroslavl, Russia).

apparently magmatic ones. The latter include magnesian phlogopite (1 and 6 in Table 4), which is found as small scattered plates in the harzburgite (1.6–2.3 wt% TiO_2, Mg# 93.2–93.7), and low-Cr and high-Na (0.2–0.6 wt% Cr_2O_3 and 1.5–1.6 wt% Na_2O), and also ferroan (Mg# 56-82) biotites from diorite veinlets (4, 5, 7 in Table 4) showing a high Ti content (2.6 wt% TiO_2) and a low Cr content (0.0–0.10 wt% Cr_2O_3). These biotites are close to the biotites described from the gabbroid and gabbro veinlets cutting oceanic peridotites [*Cannat and Casey,* 1995; *Silantiev,* 1998].

In terms of the Ti content the hornblendes can be classified into high-Ti, supposedly magmatic ones (1.3–2.7 wt% TiO_2) and low-Ti hornblendes (<0.7 wt% TiO_2), supposedly of nonmagmatic origin. High-Ti hornblende occurs as scattered grains in the hartzburgite (1–4 and 7 in Table 2), is associated with high-Ti phlogopite and orthopyroxene, and is distinguished by its high magnesium number (Mg# 91.6–92.5), high Cr contents (0.5–2.0 wt% Cr_2O_3), and rather high K contents (0.36–0.54 wt% K_2O). The primary brown magmatic hornblende, found in diorite veinlets, has a low Mg number (Mg# 53-58), a high Ti content (2.4 wt% TiO_2), and an elevated K content (0.41–0.47 wt% K_2O) with an almost absent chromium.

The orthopyroxenes from the harzburgite (14 and 15 in Table 1), associated with high-Ti hornblende and phlogopite, are low in alumina (1.1–1.4 wt%), Cr (0.2–0.3 wt% of oxide), and Ca (0.5–0.8 wt% of oxide), and are notably enriched in Ti (0.22–0.25 wt% of oxide) relative to the primary orthopyroxene, but do not show any difference from the latter in Mg#. The crystallization temperature of these pyroxenes was found, using a Ca-orthopyroxene geothermometer [*Brey and Köhler,* 1990], to be not lower than 870–950°C (Table 1). The temperature of pyroxene crystallization in the gabbro veinlets was found by a number of geothermometers to be close to 1000°C (Table 1).

Compared to the low-Ti chrome spinellids, typical of restite peridotite, there are spinellids that are highly enriched in Ti (>0.6 wt% TiO_2), associated with high-Ti amphiboles. In some cases (10 in Table 3) these are grains concentrated in a gabbro-harzburgite contact, in other cases (4 in Table 3) the grains are localized in the middle of the amphibole veinlet.

REE and trace elements. The REE contents are highly variable in the hornblende (Table 5, Figure 1) differing by more than 100 times. The hornblende from the diorite veinlets showed the highest REE contents ($Yb_N \sim 600$, $(La/Yb)_N = 0.56$) (hereinafter N denotes the contents normalized to chondrite after [*Anders and Grevesse,* 1989]). It is comparatively low in the most light and most heavy REE relative to Sm and has a negative Eu anomaly. The high-Ti hornblende of the harzburgite is lower in REE and yielded the more flat spectra of a normalized REE distribution: $(La/Sm)_N = 0.5–1.0$ and $(Sm/Yb)_N = 1.35–1.65$ with higher Ce and Nd contents and a characteristic negative Eu anomaly. The hornblende from the diorite showed pronounced Sr, Ba, Ti, and Zr negative anomalies (Figure 2). The high-Ti hornblende of the harzburgite showed the same anomalies except for the zircon one.

None of the pyroxenes analyzed using an ion microprobe (Table 5) showed an equilibrium with hornblende. The clinopyroxenes yielded even spectra with obvious indications

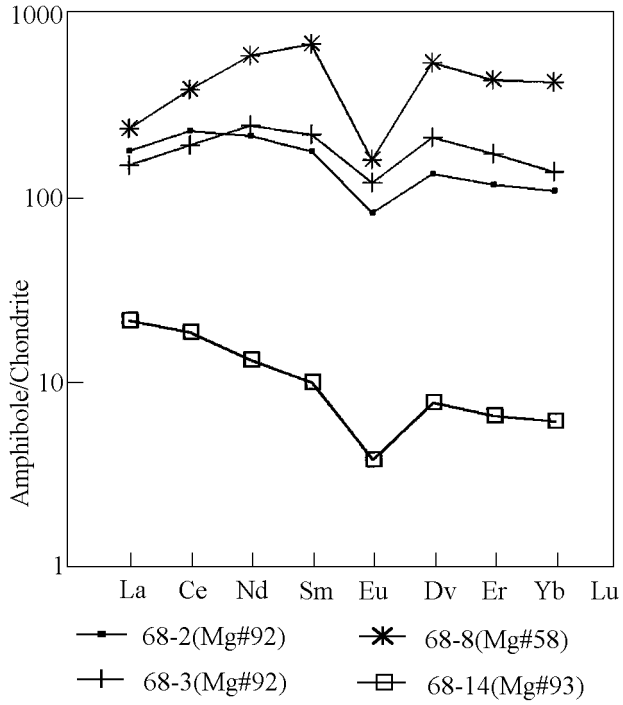

Figure 1. Distribution of chondrite-normalized REE contents in hornblendes from MAR peridotites.

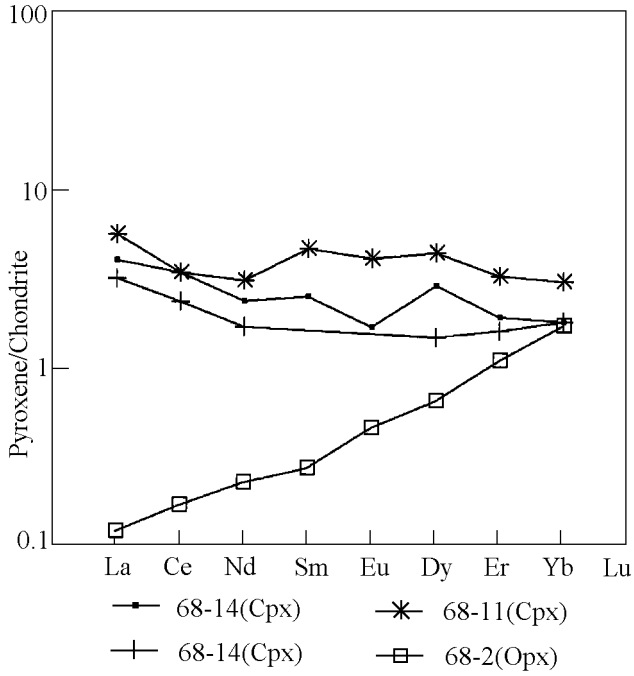

Figure 3. Distribution of chondrite-normalized REE contents in pyroxenes from the spinel peridotite of dredge sample 68.

of LREE enrichment (Figures 3 and 4). The orthopyroxenes were found to be depleted in MREE and HREE, except for those from the harzburgite of dredge sample 62, which are enriched in LREE. The clinopyroxenes also showed negative Ti, Zr, Sr, Nb, and Ba anomalies.

The orthopyroxenes yielded a positive Li anomaly, those from dredge sample 68 being characterized by negative Sr and Ba anomalies, and those from dredge sample 62, by a positive Sr and a negative Zr anomaly.

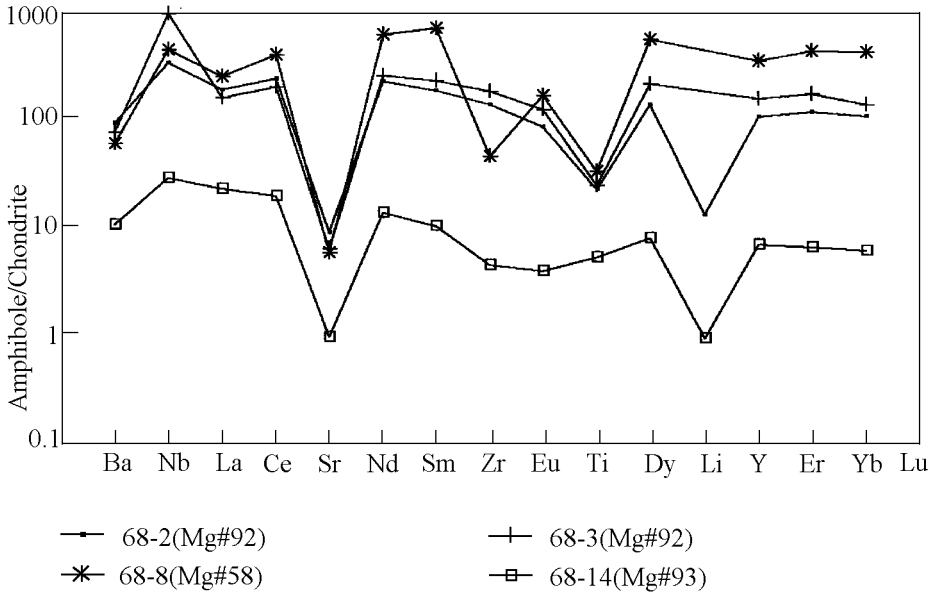

Figure 2. Distribution of chondrite-normalized trace element contents in hornblendes from MAR peridotites.

Table 6. Mineral-melt partition coefficients used

Mineral	Cpx	Opx	Hbl	Ol	Spl	Mica	Pl	Ilm
Ba	0.0003^{K}	0.0006^{D}	0.12^{F}	0.0005^{D}	0.0005^{D}	3.68^{H}	0.13^{J}	0.01^{D}
Nb	0.0077^{D}	0.004^{D}	$0.15^{B,H}$	0.01^{D}	0.01^{D}	0.088^{H}	0.01^{C}	2.3^{D}
La	0.035^{A}	0.0025^{A}	0.12^{A}	0.000007^{A}	0.0006^{A}	0.0006^{M}	0.27^{C}	0.0072^{D}
Ce	0.055^{A}	0.005^{A}	0.18^{A}	0.00001^{A}	0.0006^{A}	0.0006^{B}	0.20^{C}	0.00783^{D}
Sr	0.065^{A}	0.01^{A}	0.16^{A}	0.00019^{A}	0.0008^{A}	0.085^{L}	2.0^{C}	0.7^{D}
Nd	0.15^{A}	0.01^{A}	0.49^{A}	0.00007^{A}	0.0006^{A}	0.0006^{B}	0.14^{C}	0.00847^{D}
Sm	0.25^{A}	0.02^{A}	0.69^{A}	0.0007^{A}	0.0006^{A}	0.0008^{B}	0.11^{C}	0.0091^{D}
Zr	0.15^{A}	0.07^{A}	0.41^{A}	0.007^{A}	0.07^{A}	0.017^{H}	0.014^{C}	0.4^{D}
Eu	0.32^{A}	0.03^{A}	1.00^{A}	0.00095^{A}	0.0006^{A}		0.73^{C}	0.0084^{D}
Ti	0.23^{A}	0.15^{A}	0.99^{A}	0.015^{A}	0.15^{A}	1.37^{L}	0.04^{C}	16^{D}
Dy	0.35^{A}	0.05^{A}	0.98^{A}	0.004^{A}	0.002^{A}	0.0045^{B}	0.055^{C}	0.0106^{D}
Li	0.27^{E}	0.20^{E}	0.19^{E}	0.35^{E}		0.064^{H}	0.151^{G}	
Y	0.37^{A}	0.06^{A}	1.18^{A}	0.0065^{A}	0.0023^{A}	0.007^{I}	0.050^{M}	0.0045^{D}
Er	0.37^{A}	0.07^{A}	0.93^{A}	0.009^{A}	0.003^{A}	0.0074^{B}	0.041^{C}	0.01625^{D}
Yb	0.37^{A}	0.08^{A}	0.86^{A}	0.023^{A}	0.005^{A}	0.007^{M}	0.031^{C}	0.02475^{D}

Note. Cpx = clinopyroxene, Opx = orthopyroxene, Hbl = hornblende, Ol = olivine, Spl = chrome spinellid, Mica = biotite/phlogopite, Pl = plagioclase, Ilm = ilmenite. References: [A] – [*Ozawa and Shimizu,* 1995]; [B] – [*Ionov et al.,* 1997]; [C] – [*McKenzie and O'Nions,* 1991]; [D] – [*Bédard,* 1994]; [E] – [*Brenan et al.,* 1998]; [F] – [Brenan et al., 1994]; [G] – [*Blundy et al.,* 1998]; [H] – [*LaTourrette et al.,* 1995]; [I] – [*Foley et al.,* 1996]; [J] – [*Grove and Kinzler,* 1986]; [K] – [*Halliday et al.,* 1995]; [L] – estimated using $D^{Hbl/melt}$ after [*Ozawa and Shimizu,* 1995] and $D^{Phl/Hbl}$ after [*LaTourrette et al.,* 1995]; [M] – estimate based on the values of partition coefficients for elements similar in the degree of incompatibility.

Estimation of Equilibrium Between Mineral Phases and Coexisting Melts

The calculations discussed below were made using the coefficients of the partition of elements between the minerals and the melt, given in Table 6. As mentioned above, the solidus association in the studied harzburgites was a paragenetic sequence of Ol+OpxS+Spl, with clinopyroxene and hornblende crystallization taking place at subsolidus temperature. Nevertheless, where the difference in the values of the partition coefficients of elements between the minerals (Opx/Cpx, Opx/Hbl) was low (which is a universally accepted fact now), and where the system was closed to the addition of elements during the subsolidus crystallization of clinopyroxene and hornblende (as has been demonstrated above by the calculation of a mass balance for the case of clinopyroxene crystallization through the exsolution of solidus orthopyroxene, reaction (4)), then the melt compositions calculated from the mineral/melt partition coefficients, equiponderant with the compositions of the subsolidus pyroxenes, must be close to the composition of a melt which was in equilibrium with the solidus orthopyroxene. This is illustrated in Figure 5 which compares the compositions of the melts which were in equilibrium with the subsolidus clinopyroxene of Sample 68-14 and with the solidus orthopyroxene, the composition of which was reconstructed using a mass balance equation (4).

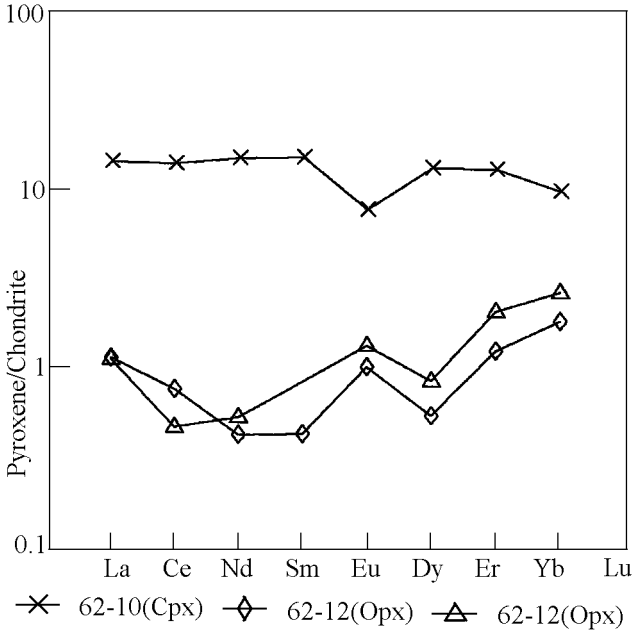

Figure 4. Distribution of chondrite-normalized REE contents in pyroxene from the spinel peridotite of dredge sample 62.

Since the reactions of metamorphic amphibolization imply the obligatory addition of sodium in the course of this process, even where the system was closed to the addition of major elements (reactions (5) and (6)), a conformity between the composition of the melt, equiponderant with the pyroxenes from the same sample, generally requires an additional confirmation.

In order to estimate the degree of equilibrium between the coexisting minerals (which is important for elucidating the origin of hornblende) and the degree of the heterogeneity of melts for the rocks of the same type, dredged from the same site, we compared the compositions of some hy-

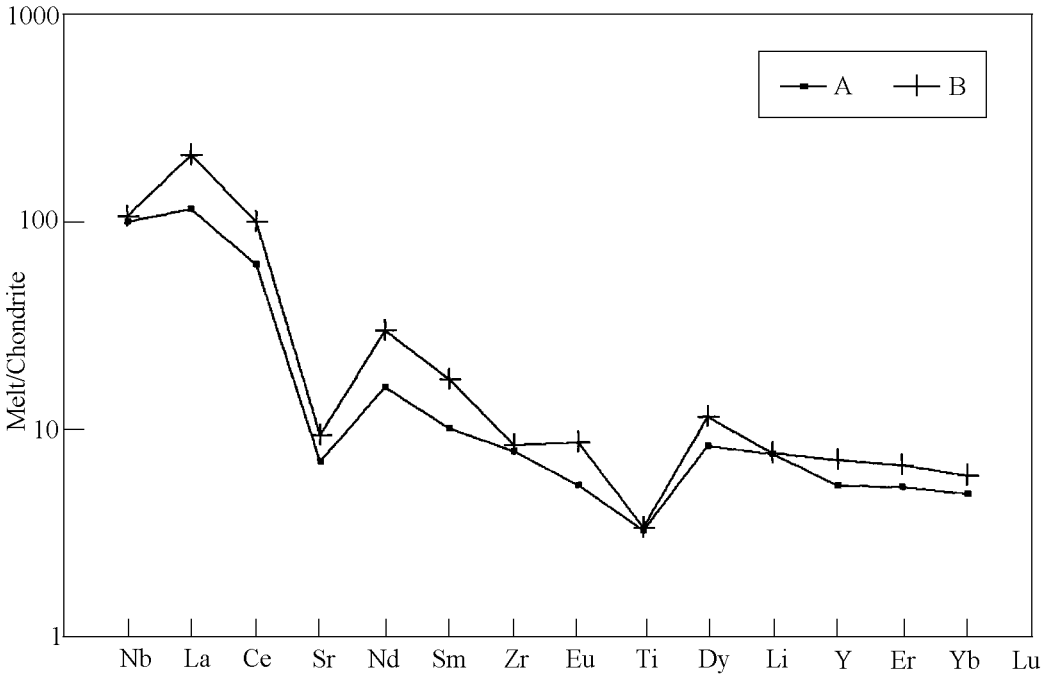

Figure 5. Effect of the subsolidus recrystallization of peridotite on the calculated composition of magma in equilibrium with peridotite minerals. A – composition of magma in equilibrium with the measured composition of subsolidus clinopyroxene 68-14; B – composition of magma in equilibrium with the calculated composition of solidus orthopyroxene.

pothetical melts supposed to be in equilibrium with different minerals. The compositions of the melts found to be in equilibrium with the orthopyroxenes and clinopyroxenes of the harzburgite from dredge sample 68 are rather similar (Figure 6). The incomplete coincidence of the compositions is the accumulated effect of analytical errors and the not full correspondence of the mineral-melt partition coefficients for different minerals. It is possible that this circumstance reflects the real variations in the compositions of the last melt portions that had separated from different samples collected by the same dredge, because some differences in the compositions of the primary minerals suggest variations in the partial melting degree for the peridotites from the same dredge sample. It is important that the composition of the melt found to be in equilibrium with the low-Ti hornblende from the harzburgite corresponds, in terms of the contents of all elements, to the composition of the melt which was in equilibrium with the pyroxenes. Therefore this fact suggests the absence of any essential addition of REE and trace elements during the metamorphic crystallization of low-Ti hornblende, at least in the case discussed.

The calculated compositions of the melts that were in equilibrium with orthopyroxenes and clinopyroxenes from the harzburgite of Sample 62 are also rather similar (Figure 7). The compositions of the melts that were found to be in equilibrium with the low- and high-Ti hornblendes from this hartzburgite are markedly different both from one another and from the composition of the melt which was in equilibrium with the pyroxenes. This suggests that both hornblendes were not in chemical equilibrium with the pyroxenes and could not crystallize without a significant addition or removal of some REE and trace elements. Therefore the compositions of these amphiboles cannot be used to reconstruct the magmatic history of the peridotites.

The calculated compositions of the melts that were in equilibrium with hornblende and biotite from a diorite veinlet are similar in terms of the Ba, Nb, Sr, and Ti contents (Figure 8), which suggests a chemical equilibrium of these minerals, which can also be inferred from the structural relations between them. The compositions of the melts are slightly different in terms of the Ce, Yb, Y, and Zr contents. This might have stemmed from the high error of determining the contents of these elements in mica because of their low concentrations, or from the high uncertainty of the biotite/melt distribution ratio for these elements.

The above data suggest that the average composition of the melts that were in equilibrium with clinopyroxenes 68-11 and 68-14 and with hornblende 68-14 (2, 3, and 7 in Table 5) represents the composition of the last portion of the melt that separated from the harzburgite of dredge sample 68. Similarly, the average melt that was in equilibrium with clinopyroxene 62-10 and orthopyroxene 62-12 (12 and 13 in Table 5) can be taken as the last portion of the melt that separated from the harzburgite of dredge sample 62. It appears that these melts were generated in the course of global decompression melting in the mantle column that rose under the Mid-Atlantic Ridge in the area of 14–15°N, because most of the primary minerals in the studied peridotites reflect a

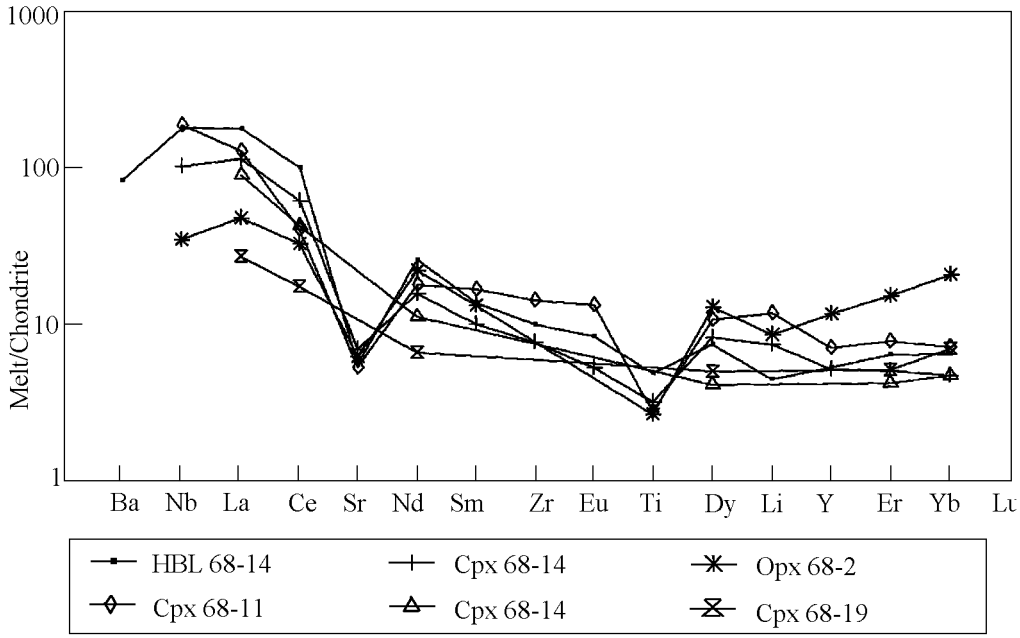

Figure 6. Calculated compositions of magma in equilibrium with different minerals of peridotite from dredge sample 68.

chemical equilibrium with the melts that are characterized by similar geochemical parameters. These model melts can be classified as the principal ones; they are labeled as M68-1 and M62-1 in Table 7.

The compositional similarity of high-Ti hornblendes in the harzburgites of Samples 68-2 and 68-3, suggests, along with their high Ti contents, that the mean composition of the melts which were in equilibrium with these amphiboles (5 and 6 in Table 5) was close to the composition of a hypothetic melt that "oozed" through the still hot, though solidified peridotite. Further, it can be assumed that the mean composition of the melt, calculated on the assump-

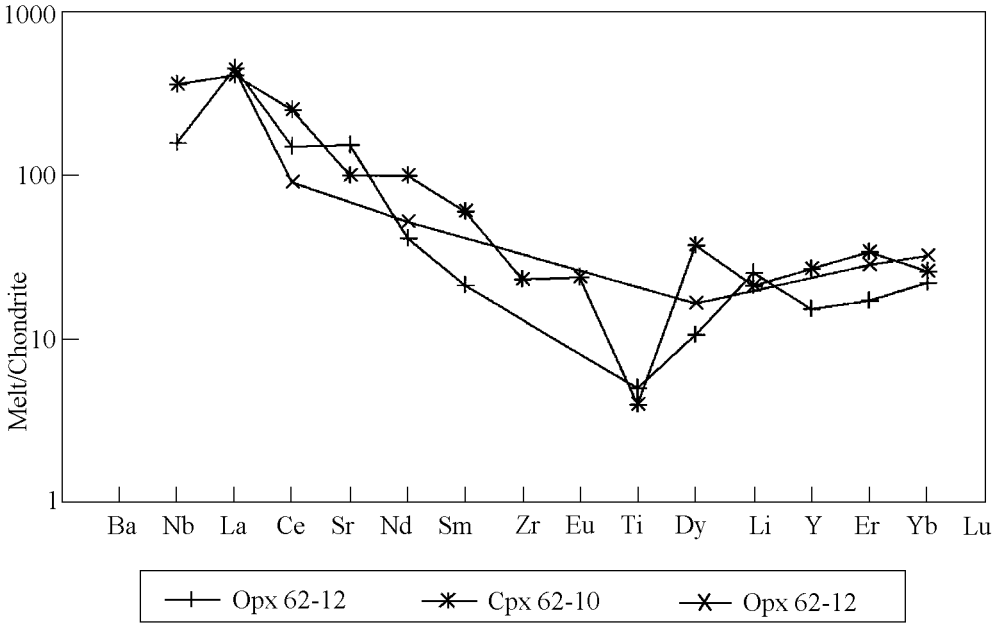

Figure 7. Calculated compositions of magma in equilibrium with different minerals of peridotite from dredge sample 62.

Table 7. Compositions of representative melts associated with the MAR peridotites examined

Melt	M68-1	M68-2	M68-3	M62-1
Ba	194	1535	1183	ND
Nb	33	856	668	58
La	32	317	457	100
Ce	39	693	910	118
Sr	47	350	290	978
Nd	9.1	212	539	30
Sm	2.0	42	143	5.4
Zr	42	1451	245	93
Eu	.5	5.5	8.9	1.6
Ti	1615	9966	10500	2021
Dy	2.2	42	132	5.1
Li	12	102	536	37
Y	9.8	169	457	34
Er	1.1	24	73	4.1
Yb	1.1	23	78	4.1
$(La/Sm)_N$	10.1	4.7	2.0	11.7
$(La/Yb)_N$	20.8	9.6	4.0	16.7
$(Sm/Yb)_N$	2.1	2.0	2.0	1.4

Note. The ratios of RRE contents were chondrite normalized. The contents of all elements are given in ppm, ND – not determined.

tion of equilibrium with the hornblende and biotite from a diorite veinlet in Sample 68-8 (8 and 9 in Table 5), reflects the composition of the melt that was intruded into the already relatively cold peridotite. Both of these melts (M68-2 and M68-3 in Table 7) were undoubtedly intruded later than the main melt, and their effect on the compositions of the primary minerals of the peridotite was limited and local.

To clarify the potential relationships among the different melts, associated with the peridotite of dredge sample 68, we undertook numerical modeling for the process of fractional crystallization. Since the contents of petrogenic elements in the melts were unknown, we assumed that a relation between the fractions of the crystallizing minerals remained constant throughout the process. Also, because our modeling was based only on the contents of REE and trace elements, the distribution of the portions of olivine and orthopyroxene, as well as of ilmenite and rutile, can be admitted to be rather unreliable. Nevertheless, the results of our calculations suggest that the melt (M68-2) that "seeped" through the peridotite might have been a derivative from the main melt (M68-1) after its 96-percent fractional crystallization for the following relations among the crystallizing phases (wt.%)

$$0.376\ \mathrm{Ol} + 0.396\ \mathrm{Opx} + 0.127\ \mathrm{Pl} + \\ + 0.082\ \mathrm{Hbl} + 0.052\ \mathrm{Bi} + \\ + 0.007\ \mathrm{Ilm} - 0.308\ \mathrm{Cpx}\ . \qquad (7)$$

Similarly, the injected melt (M68-3) might have been derived from the main melt (M68-1) after its 97.7% fractional crystallization with the following relation among the crystallizing phases (wt.%)

$$0.048\ \mathrm{Ol} + 0.713\ \mathrm{Opx} + 0.150\ \mathrm{Pl} + \\ + 0.068\ \mathrm{Hbl} + 0.062\ \mathrm{Bi} + \\ + 0.007\ \mathrm{Ilm} - 0.522\ \mathrm{Cpx}\ . \qquad (8)$$

As has been mentioned above, the ilmenite fraction night have included rutile in the case of its crystallization. While calculating equation (8), we did not attempt to calculate the fractions of apatite and zircon, which had crystallized along with the other minerals. Accordingly, we neglected Zr contents in the melts. On the whole, the results of our calculations demonstrated the possibility of the magmatic crystallization of high-Ti hornblende and biotite on the condition of the high fractional crystallization of the primary melts.

Discussion of Results

Magmatic Mica and Hornblende in Mantle Peridotites.

In the studied spinel peridotites magmatic hornblendes and micas crystallized in two associations: in magmatic veinlets (association Hbl+Bi+Pl±Opx+Zr+Ilm+Ap, where hornblende is represented by edenite, and silicates are distinguished by low Mg# values), and in scattered grains as traces of melt permeation (association Hbl+Phl+Opx±Ru, hornblende is represented by pargasite or edenite, the silicates are distinguished by high Mg# values, controlled by the Mg# of the silicates in the host harzburgite, the typical features being the small size and small amount of hydrous silicate grains).

In both cases the hornblendes and micas are high in Ti

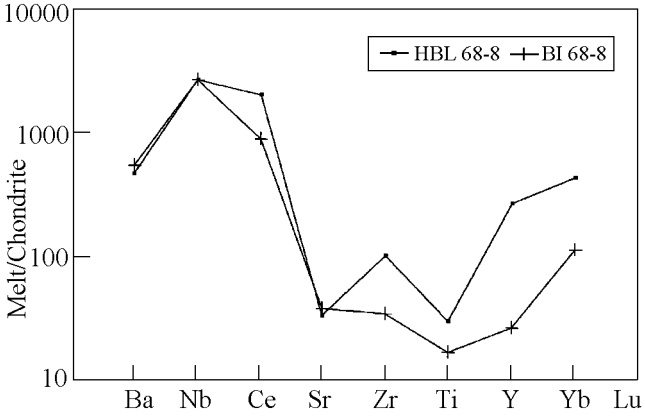

Figure 8. Calculated compositions of magma in equilibrium with different minerals of a diorite vein in peridotite from dredge sample 68, chondrite-normalized.

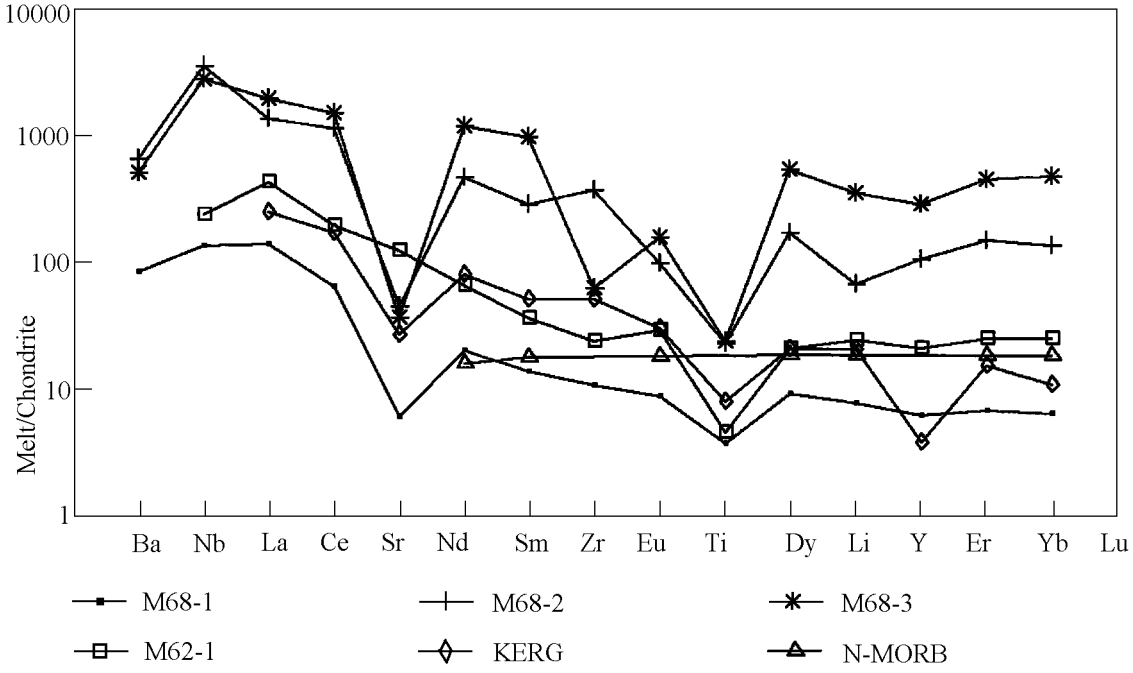

Figure 9. Comparison of the representative compositions of magmas associated with the studied peridotites (Table 7) with the mean composition of N-MORB magma [*Sun and McDonough,* 1989] and representative OIB magma (homogenized melt inclusion in olivine from a spinel peridotite xenolith of Kergelen Island [*Schiano et al.,* 1994].

(>0.9 wt.% TiO_2), the hornblendes being invariably high in alumina. The compositional variations of these minerals are mainly related to their Mg# values which, in turn, are controlled by the extent of the chemical readjustment of the melt equilibrium with the minerals of the host harzburgite (a trend of the melt Mg# buffering by the host peridotite, poorly manifested in the case of diorite veinlets and quite obvious in the case of the scattered hornblende-phlogopite mineralization).

The parameters of magmatic mica and hornblende crystallization in the different associations of spinel peridotite are fairly close. The crystallization temperature, estimated mainly from the Ca content in orthopyroxene (Table 1) was not lower than 870–950°C but not higher than 1000°C. The pressure during the crystallization of these minerals seems to have been not higher than 6 kbar: the pressure of the principal melt separation from spinel harzburgite was estimated in [*Bazylev and Silantiev,* 2000] to be 6.3 kbar. The oxygen fugacity during the crystallization of these minerals was somewhat higher than that of the enclosing mantle spinel peridotite, but was not higher than the fugacity 1.2 logarithmic units higher than the QFM buffer (Table 3).

The crystallization of magmatic hornblendes and micas in the peridotite was spatially associated with the crystallization, in the same rocks, of amagmatic hornblendes and phlogopites, the main difference of which is the low Ti content. The problem of the genesis of these minerals is beyond the scope of this paper.

Main characteristics of peridotite-related melts.

The spatial restriction of the phlogopite mineralization in MAR spinel peridotite to the area of the 14°48′ N geochemical anomaly seems to be not accidental. Apparently the presence of magmas enriched in potassium and water, typical of this MOR region [*Sobolev et al.,* 1992], was a significant factor for phlogopite and hornblende crystallization in the peridotite.

It should be noted that mineral/melt partition coefficients for trace elements and especially for REE, as well as plagioclase/melt coefficients for Ba and Sr, depend on the contents of silica and alumina in the melt [*Bédard,* 1994; *Ionov et al.,* 1994; *Vannucci et al.,* 1998]. Since the contents of petrogenic elements in the melts were not determined in this study, calculations were made using some constant values of the partition coefficients, which led to errors and to the semiquantitative character of modeling magmatic melt fractional differentiation.

The principal melts that separated from the harzburgites of dredge samples 68 and 62 were enriched in LREE and showed comparable values of the chondrite-normalized ratios $(L/Sm)_N$ (10–12) and $(Sm/Yb)_N$ (2.0–2.1), but differ slightly in the HREE contents, in particular, in Yb_N (7–26) (Figure 9, Table 7). These compositional features are not characteristic of the basalts and glasses of the N-MORB type, but are inherent in the compositions of some so-called

ultrarich melt inclusions in olivines from the basalts of this MAR region [*Sobolev,* 1997], which showed the $(La/Sm)_N$ value to be 11.3 [*Tsameryan et al.,* 2000]. The high enrichment of the basic magmas in light rare-earth elements agrees with the LREE-rich clinopyroxenes in the spinel harzburgite, devoid of hornblende and mica, dredged from the neighboring MAR areas [*Dick and Kelemen,* 1992].

The melt which seeped through the peridotite and from which high-Ti and high-Mg hornblende and phlogopite crystallized in the spinel harzburgite of dredge sample 68 was enriched in HREE ($Yb_N = 140$), which suggests the high degree of its differentiation. The intensive fractional crystallization is emphasized also by the negative Sr and Ti anomalies, indicative of plagioclase and rutile crystallization.

The melt that was injected into the peridotite of dredge sample 68, from which the minerals of the diorite veinlets, including hornblende and biotite, crystallized, was even more enriched in medium and heavy REE ($Yb_N = 480$) and showed, in addition to negative Ti and Sr anomalies (apparently caused by ilmenite and plagioclase crystallization), a negative Zr anomaly proving zircon crystallization. Therefore the absence of a negative Zr anomaly in the injected melt suggests that the high-Ti and high-Mg amphibole and phlogopite crystallized in the peridotite prior to the diorite magma intrusion into it.

Although the calculated modes of minerals during their fractional crystallization are semi-quantitative values, the negative value of the mode for clinopyroxene suggests that the crystallization of olivine, orthopyroxene, plagioclase, hornblende, biotite, and ilmenite from the melt was accompanied by the dissolution of clinopyroxene, more active than its crystallization imprinted in the gabbro veinlets. The extremely high value of a mode for the dissolved clinopyroxene seems to have been caused by the assumption of a chemical equilibrium between clinopyroxene and magma (meaning the dissolution of accumulative clinopyroxene from the gabbro veinlets). The more probable mechanism, however, seems to be the dissolution of the dispersed clinopyroxene from the peridotite during the early phases of magma fractionation (or of the subsolidus clinopyroxene, derived from orthopyroxene, which is highly enriched in LREE). In this case the dissolving clinopyroxene might have been in disequilibrium with the magma, and its quantity might have been significantly lower than that which follows from the assumption of its equilibrium.

In any case, in the long run, the crystallization of mica and amphibole in the peridotite seems to have been associated with the saturation of the residual melts with water, K, and Na because of the high degree of their fractional crystallization, that is, with the mechanism proposed earlier by [*Arai and Matsukage,* 1996; *Arai et al.,* 1997].

The source of water and incoherent elements.

It is important that magmatic mica was introduced into the mineral association during the late phase of the magma fractional crystallization, by the time when the peridotite had cooled off to a temperature below the solidus one. For instance, in Sample 68-37 biotite is absent from the gabbronorite association of the veinlet middle (Cpx-Opx-Pl), but appears in the more differentiated diorite veinlets (in this and other samples), where clinopyroxene is no longer present (Opx-Pl-Hbl-Bi).

Therefore the mica and hornblende of the investigated spinel harzburgite cannot be regarded as the potential sources of water and incoherent elements, their crystallization marking the end of the magmatic process.

Nevertheless, this does not remove the problem of the source of water and incoherent elements, including the crystallization of the hydrous silicates described. It is remarkable that the compositions of the principal magmas calculated for the harzburgites of dredge samples 68 and 62 show an obvious similarity with the compositions of OIB-type basaltoids, in particular, with the homogenized melt inclusions in the olivine from the peridotite xenoliths in the basalts of Kerguelen I. [*Schiano et al.,* 1994]. The composition indications of the calculated magmas of types E-MORB or OIB agree with the location of dredging sites 62 and 68 in the vicinity of the 14°48′ N geochemical anomaly, the largest in the Central Atlantic [*Sobolev et al.,* 1992]. Moreover, it was in the MAR segment, immediately south of the 15°20′ N fracture zone, where dredging site 68 was located, that the presence of mantle peridotites, isotopically corresponding to the enriched subcontinental lithospheric mantle, was established [*Silantiev et al.,* 2001].

The compositions of the principal magmas, determined in this study for the spinel peridotite from dredge samples 62 and 68, suggest that (1) the enrichment of the mantle magmas in incompatible elements was of a regional type (as follows from the above-mentioned similarity of the La/Sm and Sm/Yb ratios in them) and (2) their Sr anomaly is of mantle origin.

The mantle origin of the Sr anomaly in the magmas was earlier interpreted as the evidence of the recycling of the oceanic lithosphere material – of its sinking in subduction zones and rising in regions of plume activity [*Sobolev et al.,* 2000]. These researchers interpreted the positive Sr anomaly in some melt inclusions as the consequence of the melting of eclogite derived from a plagioclase-rich layer of oceanic gabbro.

The M68-1 magma showed a high negative Sr anomaly, the origin of which can therefore be associated with the selective melting of eclogite which developed after the plagioclase-poor accumulative gabbro. The absence of a Sr anomaly in the M62-1 magma agrees with the view advanced in [*Sobolev et al.,* 2000] on the local character of the source and on the type of a Sr anomaly in regions of plume-type magma generation.

Conclusions

1. The high-Ti magmatic hornblende and mica from the MAR spinel harzburgite crystallized from residual, highly differentiated (96–98%) mantle magmas or during their interaction with the host mantle material at temperatures of 870–950°C.

2. The calculated initial mantle magmas, which were in equilibrium with the minerals of the restite harzburgite, agree, in terms of their enrichment in LREE (La/Sm_N = 10–12), with intraplate magmas, from which basalts of the OIB type were derived.

3. The absence of a Sr anomaly in the model composition of the source magma, estimated for one of the two MAR regions under study (site 16 ABP-68), and a negative Sr anomaly typical of the model magma composition, calculated for the other area of the ridge (site 16 ABP-62), can be interpreted as the independent confirmation of the local material heterogeneity of intraplate magma generation regions, possibly associated with the recycling of the crust material.

Acknowledgments. We are grateful to S. G. Simakov (Institute of Microelectronics, Yaroslavl) and to P. Kelemen (Woods Hole Oceanographic Institution) for their help in ion microprobe operations and to K. I. Ignatenko (GEOCHI RAN) for his help in electron microprobe measurements. We are thankful to Portnyagin M. V. (GEOCHI RAN) for his discussion of the models that involved the use of mineral-melt element partition coefficients. Thanks are also due to A. Zanetti and R. Vannicci for their constructive comments on this paper. This study was supported by the Russian Foundation for Basic Research (RFBR), project no. 00-05-64165, and by the RFBR grant for the young scientists of the Academy.

References

Anders, E., and N. Grevesse, Abundances of the elements: Meteoric and solar, *Geochim. Cosmochim Acta, 53,* 197–214, 1989.

Arai, S., and T. Fujii, Petrology of ultrabasic rocks from Site 395, in *Initial Reports of DSDP, 45,* pp. 587–594, Melson W. G., et al. (Eds.), Washington (US Govt. Printing Office), 1978.

Arai, S., and K. Matsukage, Petrology of gabbro-troctolite-peridotite complex from Hess Deep, Equatorial Pacific: Implications for mantle-melt interaction within the oceanic lithosphere, in: *Proceedings of ODP, Scientific Results, 147,* pp. 135–148, Mevel C. et al. (Eds.), College Station, TX (Ocean Drilling Program), 1996.

Arai, S., K. Matsukage, E. Isobe, and S. Vysotskiy, Concentration of incompatible elements in oceanic mantle: Effect of melt/wall interaction in stagnant or failed melt conduits within peridotite, *Geochim. Cosmochim. Acta, 61,* 671–675, 1997.

Ballhaus, C., R. F. Berry, and D. H. Green, High-pressure experimental calibration of the olivine-orthopyroxene-spinel oxygen geobarometer: Implications for the oxidation state of the upper mantle, *Contrib. Mineral. Petrol., 107,* 27–40, 1991.

Bazylev, B. A., S. A. Silantiev, and N. N. Kononkova, Phlogopite and hornblende in spinel harzburgites from the Mid-Atlantic Ridge: Mineral assemblages and origin, *Ofioliti, 24,* (1a), 59–60, 1999.

Bazylev, B. A., and S. A. Silantiev, Geodynamic Interpretation of the subsolidus recrystallization of mantle spinel peridotites: 1. Mid-ocean ridges, *Petrology, 8,* (3), 201–213, 2000.

Bédard, J. H., A procedure for calculating the equilibrium distribution of trace elements among the minerals of cumulate rocks, and the concentration of trace elements in the coexisting liquids, *Chem. Geol., 118,* 143–153, 1994.

Blundy, J. D., J. A. C. Robinson, and B. J. Wood, Heavy REE are compatible in clinopyroxene on the spinel lherzolite solidus, *Earth Planet. Sci. Lett., 160,* 493–504, 1998.

Brenan, J. M., E. Neroda, C. C. Lundstrom, H. F. Shaw, F. J. Ryerson, and D. L. Phinney, Behavior of boron, beryllium, and lithium during melting and crystallization: Constraints from mineral-melt partitioning experiments, *Geochim. Cosmochim. Acta, 62,* 2129–2141, 1998.

Brenan, J. M., H. F. Shaw, and D. L. Phinney, Experimental determination of trace element partitioning between pargasitic amphibole and hydrous silicate melt, *Mineral. Mag., 58A,* 121–122. 1994.

Brey, G. P., and T. Köhler, Geothermobarometry in four-phase lherzolites. II. New thermobarometers and practical assessment of existing thermobarometers, *J. Petrol., 31,* 1353–1378, 1990.

Cannat, M., and J. F. Casey, An ultramafic lift at the Mid-Atlantic Ridge: Successive stages of magmatism in serpentinized peridotites from the 15°N region, in: *Mantle and Lower Crust Exposed in Oceanic Ridges and in Ophiolites,* pp. 5–34, Vissers R. L. M. and Nicolas A. (Eds.), Kluwer Acad. Publ., 1995.

Cannat, M., D. Bideau, and H. Bougault, Serpentinized peridotites and gabbro in the Mid- Atlantic Ridge axial valley at 15°37′ N and 16°52′ N, *Earth Planet. Sci, Lett., 109,* 87–106, 1992.

Dick, H. J. B., Abyssal peridotites, very slowly spreading ridges and ocean ridge magmatism, in: *Magmatism in Ocean Basins,* pp. 71–105, Sounders A. D. and Norry M. J. (Eds.), London, Geol. Soc. Spec. Publ., 42, 1989.

Dick, H. J. B., and P. B. Kelemem, Light LREE-enriched clinopyroxene in harzburgite from 15°05′ N on the Mid-Atlantic Ridge, *EOS Transactions, 73,* 584, 1992.

Foley, S. F., S. E. Jackson, B. J. Fryer, J. D. Greenough, and J. A. Jenner, Trace element partition coefficients for clinopyroxene and phlogopite in an alkaline lamprophyre from Newfoundland by LAM-ICP-MS, *Geochim. Cosmochim. Acta, 60,* 629-638, 1996.

Fujii, T., Petrology of peridotites from Hole 670A, Leg 109, *Proc. ODP Scientific Results, 106/109,* 19–25, 1990.

Grove, T. L., and R. J. Kinzler, Petrogenesis of andesites, *Annual Rev. Earth Planet. Sci., 14,* 417–454, 1986.

Hamlin, P. R., and E. Bonatti, Petrology of mantle-derived ultramafics from the Owen fracture zone, northwest Indian Ocean: Implications for the nature of the oceanic upper mantle, *Earth Planet. Sci. Lett., 48,* 49–65, 1980.

Halliday, A. N., D. C. Lee, S. Tommasini, G. R. Davies, C. R. Paslick, J. G. Fitton, and D. E. James, Incompatible trace elements in OIB and MORB and source enrichment in the suboceanic mantle, *Earth Planet. Sci. Lett., 133,* 379–395, 1995.

Ionov, D. A., W. L. Griffin, and S. O'Reilly, Volatile-bearing minerals and lithophile trace elements in the upper mantle, *Chem. Geol., 141,* 153–184, 1997.

Ionov, D. A., A. W. Hofmann, and N. Shimizu, Metasomatism-induced melting in mantle xenoliths from Mongolia, *J. Petrol., 35,* 753–785, 1994.

Johnson, K. T. M., H. J. B. Dick, and N. Shimizu, Melting in the oceanic upper mantle: An ion microprobe study of diopsides in abyssal peridotites, *J. Geoph. Res., 95,* 2661–2678, 1990.

Juteau, T., E. Berger, and M. Cannat, Serpentinized residual mantle peridotites from the MAR median valley, ODP Hole 670A (21°10′ N, 45°02′ W, Leg 109): Primary mineralogy and geothermometry, *Proceedings of ODP Scientific Results, 106/109,* 27–45, 1990.

LaTourrette, T., R. L. Hervig, and J. R. Holloway, Trace element partitioning between amphibole, phlogopite, and basanite melt, *Earth Planet. Sci. Lett., 135,* 13–30, 1995.

Lavrentiev, Yu. G., L. N. Pospelova, and N. V. Sobolev, Determination of the compositions of rock-forming minerals by an X-ray microanalysis, *Zavodskaya Laboratoriya, 40,* 657–666, 1974.

Leake, B. E., A. R. Woodley, C. E. S. Arps, W. D. Birch, M. C. Gilbert, J. D. Grice, F. C. Hawthorne, A. Kat, H. J. Kisch, V. G. Krivovichev, K. Linthout, J. Laird, J. Mandarino, W. V. Maresch, E. H. Nickel, N. M. S. Rock, J. C. Schumacher, D. C. Smith, N. C. N. Stephenson, L. Ungaretti, E. J. W. Whittaker, and G. Youzhi, Nomenclature of Amphiboles. Report of

the Subcommittee on Amphiboles, International Mineralogical Association Commission on New Minerals and Mineral Names, *European J. Mineralogy, 9,* 623–651, 1997.

McKenzie, D., and R. K. O'Nions, Partial melt distributions from inversion of rare earth element concentrations, *J. Petrol., 32,* 1021–1091, 1991.

Ozawa, K., and N. Shimizu, Open-system melting in the upper mantle: Constraints from the Hayachine-Miyamori ophiolite, Northeastern Japan, *J. Geophys. Res., 100,* 22,315–22,335, 1995.

Schiano, P., R. Clocchiatti, N. Shimizu, D. Weis, and N. Mattielli, Cogenetic silica-rich and carbonate-rich melts trapped in mantle minerals in Kerguelen ultramafic xenoliths: Implications for metasomatism in the oceanic upper mantle, *Earth Planet. Sci. Lett., 123,* 167–178, 1994.

Shimizu, N., and S. R. Hart, Applications of the ion microprobe to geochemistry and cosmochemistry, *Earth Planet. Sci. Annual Rev., 10,* 483–526, 1982.

Silantyev, S. A., Origin conditions of the Mid-Atlantic Ridge plutonic complex at 13–17° N, *Petrology, 6,* 351–387, 1998.

Silantyev, S. A., B. V. Belyatsky, V. E. Beltenev, and I. V. Vikentyev, The distribution of isotope signatures in MAR peridotites between 12° and 36°N and two kinds of mantle substratum bellow ridge axis, *InterRidge News,* Fall issue, 2001.

Sobolev, A. V., *Problems of Mantle Magma Origin and Evolution,* Doctoral (Geol.) Dissertation, Moscow, GEOCHI RAN, 1997.

Sobolev, A. V., L. V. Dmitriev, O. P. Tsameryan, V. A. Simonov, S. G. Skolotnev, and B. A. Bazylev, The structure and origin of a geochemical anomaly in basalts of layer 2 between 12 and 18°N Mid-Atlantic ridge, *Dokl. Ross. Akad. Nauk, 326,* (3), 541–546, 1992.

Sobolev, A. V., A. W. Hofmann, and I. K. Nikogosian, Recycled oceanic crust observed in "ghost plagioclase" within the source Mauna Loa lavas, *Nature, 404,* 986–990, 2000.

Sun, S.-S., and W. F. McDonough, Chemical and isotopic systematics of oceanic basalts: implications for mantle composition and processes, in: *Magmatism in the Ocean Basins,* Sounders A. D., and Norry M. J. (Eds.), London, Geological Society Special Publication, 42, 313–345, 1989.

Tsameryan, O. P., A. V. Sobolev, N. Shimizu, E-MORB parental melts: Melt inclusions as revealed from data on melt inclusions in olivines from E-MORB at 15°N MAR, *International Conference on Melt inclusions: Sassenage, 16–18 March 2000, Abstract,* 2000.

Vannucci, R., P. Bottazzi, E. Wulff-Pedersen, E.-R. Neumann, Naturally determined REE, Y, Sr, Zr, and Ti partition coefficients between clinopyroxene and silicate melt under upper mantle conditions, *Earth Planet. Sci. Lett., 158,* 39–51, 1998.

Wells, P. R. A., Pyroxene thermometry in simple and complex systems, *Contrib. Mineral. Petrol., 62,* 129–139, 1977.

Witt-Eickschen, G., and H. A. Seck, Solubility of Ca and Al in orthopyroxene from spinel peridotite: an improved version of an empirial geothermometer, *Contrib. Mineral. Petrol., 106,* 431–439, 1991.

(Received October 11, 2001)